ORNL/TM-2017/338

Quality Optimization of Commercial FeCrAl Tube Production

Yukinori Yamamoto
Zhiqian Sun

Prepared for
U. S. Department of Energy
Office of Nuclear Energy

June 30, 2017
M3FT-17OR020202121

OAK RIDGE NATIONAL LABORATORY
MANAGED BY UT-BATTELLE FOR THE US DEPARTMENT OF ENERGY

ORNL/TM-2017/338

Fuel Cycle Research and Development, Advanced LWR Fuels

Quality Optimization of Commercial FeCrAl Tube Production

Yukinori Yamamoto, Zhiqian Sun

Date Published: June 30, 2017

Work Package Title: ATF Cladding Production
Work Package #: FT-17OR02020212
Work Package Manager: Yukinori Yamamoto
Milestone #: M3FT-17OR020202121

Prepared under the direction of the
US Department of Energy
Office of Nuclear Energy
Fuel Cycle Research and Development
Advanced LWR Fuels

Prepared by
OAK RIDGE NATIONAL LABORATORY
Oak Ridge, TN 37831-6283
managed by
UT-BATTELLE, LLC
for the
US DEPARTMENT OF ENERGY
under contract DE-AC05-00OR22725

This page intentionally left blank

CONTENTS

Page

This page intentionally left blank

LIST OF FIGURES

Figure **Page**

LIST OF TABLES

Table **Page**

This page intentionally left blank

ACKNOWLEDGMENTS

The authors are grateful to Kurt Terrani and Kory Linton of Oak Ridge National Laboratory (ORNL) for their helpful discussions and management, and to Tom Geer, Dave Harper, Greg Cox, Dustin Heidel, Daniel Moore, Kevin Hanson, Victoria Cox, Brian Sparks, Brian Hannah, and Doug Stringfield of ORNL; Jim Patterson of Sophisticated Alloys Inc.; Conrad Young of Century Tubes Inc.; Todd Leonhardt, Don Mitchel, Joe Johnson, and Randy Weld of Rhenium Alloys Inc.; Kevin Heaphy and Bill Keohane of Superior Tube Company Inc.; and Russ Fawcett, Rau Rebak, and Chuck Paone of GE/GNF for their technical supports. The time spent by Sebastien Dryepondt of ORNL in reviewing this report is also greatly appreciated.

This research was funded by the US Department of Energy's Office of Nuclear Energy, Advanced Fuel Campaign of the Fuel Cycle R&D program.

This page intentionally left blank

ABSTRACT

The objectives of this report are to summarize the various process parameters and conditions that trigger premature failures during the production steps for Generation II ATF FeCrAl seamless tubes in commercially available manufacturing processes, and to suggest optimized processing routes and parameters to improve the quality and the material yield of commercial tube production. The production process steps include (1) the heat production process, (2) the master bar production process, and (3) the tube reduction process. For heat production, not only chemical composition control but also elimination of solidification defects in the vacuum induction–melted ingot are key. A hot-isostatic press helped in reducing and eliminating the internal, preexisting cracks in the ingot, which could be a source of premature failure (e.g., crack initiation from oxide particles) in the latter part of the tube production process. The master bars were produced by a hot-extrusion process. The area reduction ratio and the extrusion temperature are key to controlling the quality of the master bars and the grain structure. Because of the limited deformation ability of FeCrAl alloys, especially at ambient temperatures, a controlled, uniform grain structure with relatively small grains (<100 μm) is required at the beginning of the tube reduction process. Furthermore, a relatively small amount of area reduction per pass, combined with controlled inter-pass annealing, is important to achieve a reduction in failure events, a highly uniform wall thickness, concentricity, and a high-quality surface finish. Based on the knowledge obtained regarding process conditions, FeCrAl tube production with optimized process parameters is currently in progress. A portion of the final tube inventory was delivered in late June 2017. Cross-sectional microstructural characterization was completed for screening the quality of as-received tubes.

This page intentionally left blank

1. INTRODUCTION

1.1 Backgrounds

The development of alloys for nuclear-grade enhanced accident-tolerant fuel (ATF) cladding targets a new, metal-based structural material for nuclear fuel cladding in light water reactors (LWRs). FeCrAl alloys were selected as candidate ATF cladding alloys based on their excellent oxidation resistance in high-temperature steam environments at up to 1475°C (resulting from sufficient amounts of Cr and Al additions) compared with industry-standard zirconium alloys, which do not have comparable high-temperature tolerances [1,2,3,4]. The oxidation resistance is a key to enhancing safety margins under severe accident conditions by limiting heat and hydrogen production, which occur when the fuel cladding reacts with steam during a severe accident [5]. Development efforts for ATF FeCrAl alloys have been pursued since FY 2013 under the Fuel Cycle Research and Development program [6]. After comprehensive evaluations of a model Fe-Cr-Al-Y alloy (Gen. I), the engineering FeCrAl alloy series (Gen. II)—consisting of Fe-(10-12)Cr-(5-6)Al-Y with minor alloying additions such as Mo, Nb, Si, Ti, C, and so on—were down-selected. The selection process was based on experimental findings demonstrating good balance between mechanical properties, oxidation resistance, irradiation resistance, weldability, and so on [7,8,9,10]. The comprehensive summary of the Gen. II FeCrAl alloy development and property evaluation can be found in previous reports [11,12,13,14].

The fuel cladding in an LWR must be a seamless tube, which is typically ~4 m in length with an outer diameter (OD) of ~10 mm. In the case of FeCrAl alloys, a wall thickness of less than 0.4 mm is suggested to reduce the potential neutronic impact compared with the current zirconium alloy cladding [15,16,17]. The FeCrAl cladding should also be structurally sound, with sufficient mechanical properties at both service temperatures and accident conditions. These requirements impose considerable technical challenges for tube fabrication processes using FeCrAl alloys. Research has been performed to achieve a balance between high-temperature performance and tube fabricability in newly developed FeCrAl alloys. Body centered cubic (BCC) Fe-based materials with Cr and Al additions typically suffer from poor ductility because of their relatively high ductile-brittle transition temperatures [18]. Microstructural stability of the refined grain or subgrain structure at high temperatures is critical to maintaining both the fabricability of the alloys during tube production and the mechanical properties of the final tube products.

1.2 Tube production of ATF wrought FeCrAl alloys

One of the program targets is to produce ATF wrought FeCrAl alloy tubes through commercially available manufacturing processes. There are two different approaches to producing a seamless thin-wall tube: tube drawing and pilgering [19,20]. The tube-drawing process is widely applied for making thin-wall tubes for various industrial applications, including architecture, boilers, petrochemical and chemical plants, nuclear and fossil energy plants, aerospace, vehicles, medical equipment, and appliances. A die and mandrel are required to reduce and control the tube OD and inner diameter (ID). Tube drawing is sometimes done under warm conditions (at up to ~300°C), depending on the die and mandrel materials, to facilitate tube deformation. Pilgering, on the other hand, was developed for manufacturing tubing with ultrathin walls for nuclear fuel cladding in the 1950s [21]. Pilgering approaches are suitable for continuous production and for making longer tubes than the tube-drawing processes produce. Pilgering involves reducing the dimensions of a long starting master tube, and pilgering operations typically require a large capital investment. Therefore, the process is not suitable for producing tubes of limited length.

Trial tube production of several different FeCrAl alloys was attempted using tube drawing. Limited total lengths of Gen. I and Gen. II FeCrAl alloy tubes were fabricated in FY 2015 and FY 2016 [13, 22]. The

results were used to narrow the alloy composition ranges to improve productivity and suggest potential causes of production failure during the process. A large amount of Gen. I FeCrAl tube (B136Y3, Fe-13Cr-6Al-0.03Y wt %) was successfully fabricated, resulting in the production of more than 500 ft of tubing [22]. Mass production of Gen. II FeCrAl alloy tubes was also initiated for C35M4 (Fe-13Cr-5Al-2Mo base) and C26M (Fe-12Cr-6Al-2Mo base). Both production runs experienced many premature failures, including pointing (tagging) failures; crack initiation/propagation along the tube axial direction; circumferential rupture; gouging that created rough surfaces; and breakage of the die and mandrel, mainly as the result of the higher deformation resistance (i.e., strength) of the Gen. II alloys compared with the Gen. I alloy. Process optimization is currently in progress in parallel with the tube reduction process, based on the feedback from the tube-drawing manufacturers.

The objective of this report is to summarize the various process parameters and conditions found to trigger premature failures during the production steps for Gen. II ATF FeCrAl seamless tubes produced via commercially available manufacturing processes. Based on the information obtained, optimized processing routes and parameters are suggested to improve the quality and the material yield of tubing produced commercially. This report also includes characterization results for a portion of the C26M tubes delivered in late June 2017.

2. TUBE PRODUCTION ROUTE AND QUALITY SPECIFICATION

The commercial tube production process flow is illustrated in Figure 1. The process can be divided into three major steps: (1) heat production, (2) master bar production, and (3) tube reduction. The target total tube length through this batch process would be in a range from several feet to 500–1000 ft. The details of each process step are described in this section.

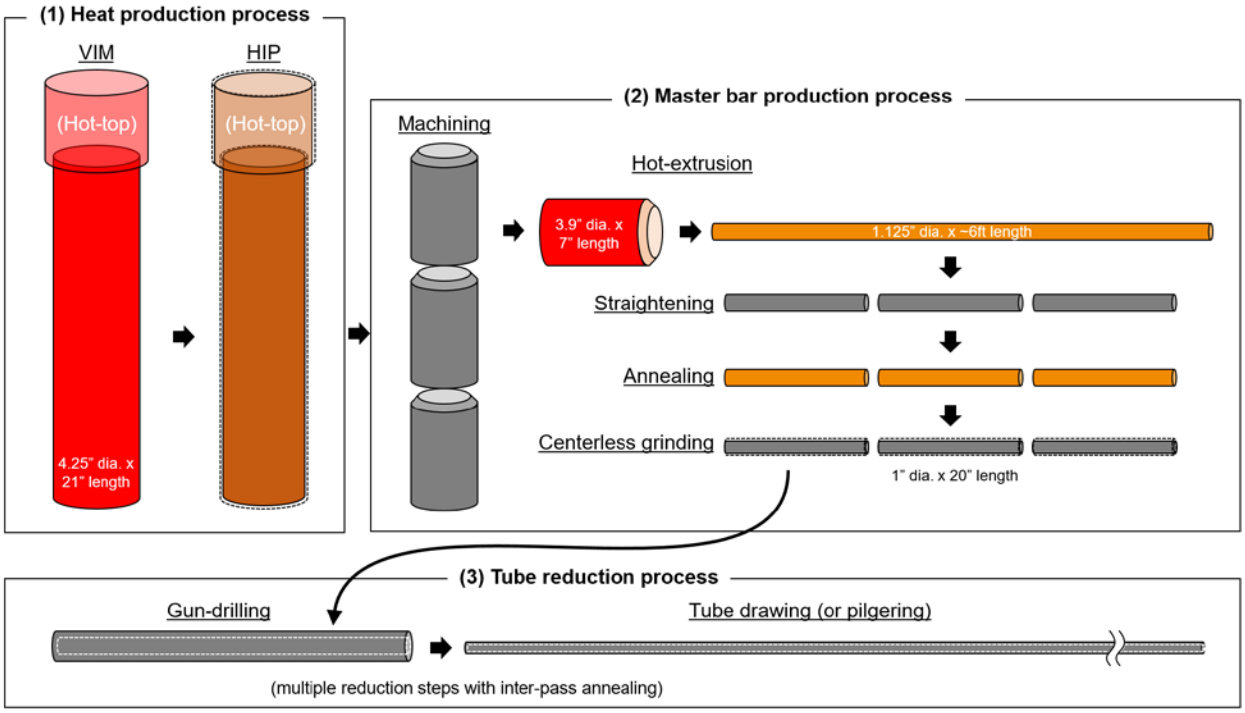

Figure 1. Tube production flow.

2.1 Heat production process

The heat production process includes vacuum induction melting (VIM) followed by hot-isostatic pressing (HIP). The specifications for the target alloy compositions should be based on the alloy design strategy, balanced with the allowable composition tolerances based on commercial melt practices. Typical target composition ranges of a Gen. II FeCrAl alloy (C26M) are shown in Table 1. A columnar shape cast ingot is made by pouring the molten metal into a graphite mold 4.25 in. diameter and 21 in. in length, together with a sufficient amount of hot-top to avoid solidification defect formation (e.g. shrinkage) at the center of the ingot. The ingot shape and size described earlier are specifically designed for subsequent master bar production through hot extrusion at ORNL, so the selection of the ingot shape/size is basically flexible and depends on the procedure that will be used for master bar production. HIP is applied for two different purposes: to eliminate internal solidification defects and to homogenize the ingot to minimize macro-segregation during solidification. It is important to apply the HIP process before sectioning the hot-top. Most solidification defects are observed as hot cracks near the center of the ingot (see Section 3.1), so the defects need to be kept to “closed pores” that do not connect to the outer surface. Otherwise, HIP cannot “heal” such defects. This process may be avoidable if the master bar production process is equivalent to HIP in terms of eliminating solidification defects and homogenizing the ingot.

Table 1. Target and analyzed alloy composition of C26M (heat #16014934)

ID		Composition,* wt %									
		Fe	Cr	Al	Y	Mo	Si	C	S	O	N
C26M	Target	Bal.	12	6	0.05	2	0.02	0.003	0.0004	0.0045	0.0003
	Max.	Bal.	12.25	6.25	0.07	2.25	0.25	0.01	0.005	0.005	0.005
	Min.	Bal.	11.75	5.75	0.03	1.75	0.15	–	–	–	–
	Analyzed	81.99	12.18	6.11	0.04	2.04	0.20	0.003	0.0004	0.0045	0.0003

* Measured by induction coupled plasma optical emission spectroscopy (most of the elements), combustion analysis (C and S), and inert gas fusion analysis (O and N).

2.2 Master bar production process

The HIPed ingot was sectioned and machined into several billets 3.9 in. diameter and 7 in. in length to match the 4-in.-diameter container sleeve in the hot-extrusion press at ORNL [22]. The size of the billets is flexible and depends on the master bar production procedure. After the billets were soaked at 900°C in argon cover gas for more than 1 h, they were extruded into a round-shape die 1.25 in. in diameter, followed by air cooling. The soaking temperature should be high enough to allow the whole billet to pass through the die with a single extrusion action, and low enough to avoid unnecessary grain coarsening by dynamic recrystallization during extrusion. It is important to minimize the temperature gradient inside the billet (nose to tail) as much as possible, since the grain size and microstructure strongly depend on the extrusion temperature. To minimize such phenomena, either heating the container sleeve or insulating the billet is effective. The argon cover gas is also optional if the soaking temperature is not significantly high and the surface oxidation is negligible. However, soaking under argon cover gas may also be helpful to avoid undesirable oxidation internally if "opened" internal cracks exist in the machined billets.

After cooling, the extruded bars were warm-straightened at a temperature range of 200–300°C, centerless ground to a 1 in. diameter, and then annealed to relieve the remaining strain and reduce the hardness for the tube reduction process. Straightening at room temperature resulted in cracking, so straightening at a warm condition was necessary. The bars were sectioned into 20 in. lengths because of the size of the furnace available for heat treatment at ORNL. The target bar diameter, length, and final annealing conditions depended on the available furnace and the tube reduction schedule.

2.3 Tube reduction process

The master bars were gun-drilled to prepare the master tubes. The wall thickness (WT) was selected in a range of 0.100–0.125 in. (± 0.002 in.) in an effort to achieve a total WT reduction of more than ~80% at the final tube production (0.136–0.157 in.) to promote refined, recrystallized grain structure. The tube drawing process was performed stepwise with a 10–17% area reduction per pass combined with inter-pass annealing in a temperature range of 800–900°C in a reduced atmosphere (e.g., hydrogen). The inter-pass annealing condition was selected to be high enough to sufficiently soften the tube for the next drawing step, and low enough to avoid undesirable grain coarsening, based on the studies previously reported [23, 24].

2.3.1 Cold/warm drawing

There are two tube drawing approaches. One uses a mandrel that moves with the drawn tube, and another uses a stationary mandrel that remains at the die end, as shown in Figure 2a and Figure 2b, respectively. The former approach minimizes the effects of inner surface friction on the tube drawing resistance, but it also requires an additional step to remove the mandrel after each drawing process step. The latter

approach directly produces the target tube size without an additional step, although the inner surface friction significantly increases the drawing resistance and often causes circumferential failure (see Section 3). Figure 2c illustrates the important parameters of the tube reduction process; OD, ID, and WT. The tube reduction steps are typically selected so as to reduce all parameters. The area reduction described in Figure 2 is controlled in a certain range (10 to 17 % for Gen. II FeCrAl alloys) to avoid the undesirable grain coarsening that occurs if the reduction ratio is too low, and to avoid premature failure resulting from exceeding the deformability of the FeCrAl alloys at room temperature. Drawing at a warm condition (~300°C) should help increase the deformability and reduce the chance of brittle fracture because that temperature is sufficiently above the ductile-brittle transition temperature of the alloy (<100°C).

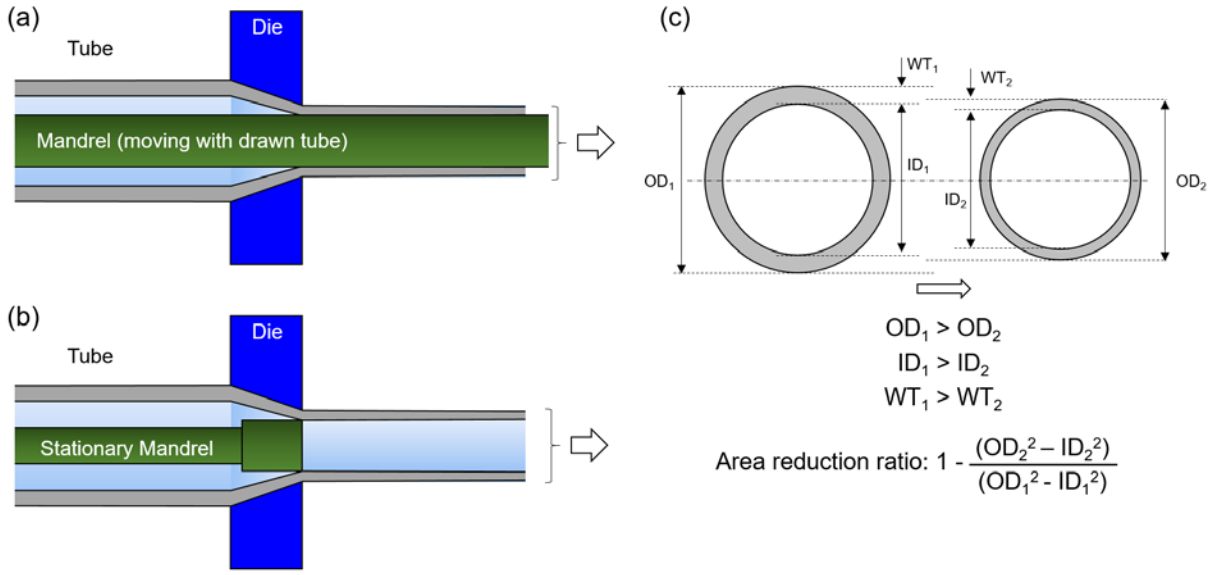

Figure 2. Illustration of tube drawing process; (a) with moving mandrel, (b) with stationary mandrel, and (c) tube size parameters for the reduction process.

2.3.2 Cold pilgering

Two main pilgering approaches are currently available, as shown in Figure 3. The high-precision tube roller (HPTR) method provides a fast, economical way to achieve extreme reductions in diameter and wall thickness. The vertical mass ring (VMR) die method uses a couple of rotating dies with varying radii for smooth tube deformation to achieve a >90% cross-sectional reduction in a single working cycle. Both pilgering approaches can be categorized as compressive production routes similar to a conventional rolling process. The HPTR and VMR methods are suitable for applying greater deformation than tube-drawing processes, although the process is not suitable for production of tubes with very limited lengths, as mentioned in the Introduction.

Although it is not within the scope of this report, a limited pilgering process was also attempted at Superior Tube Company in Germantown, Pennsylvania, using C06M2 and C36M3 tubes (Fe-10Cr-6Al-2Mo base and Fe-13Cr-6Al-2Mo base, respectively). A thickness reduction of nearly 10% was applied twice (with inter-pass annealing between reductions); it resulted in no failures and a smooth surface finish and uniform tube thickness reduction. Since compressive deformation is dominant in the pilgering process, cold pilgering is attractive for FeCrAl tube production and has the potential to significantly reduce premature failure. The production quantities it offers are suitable for this approach, and discussions are in progress.

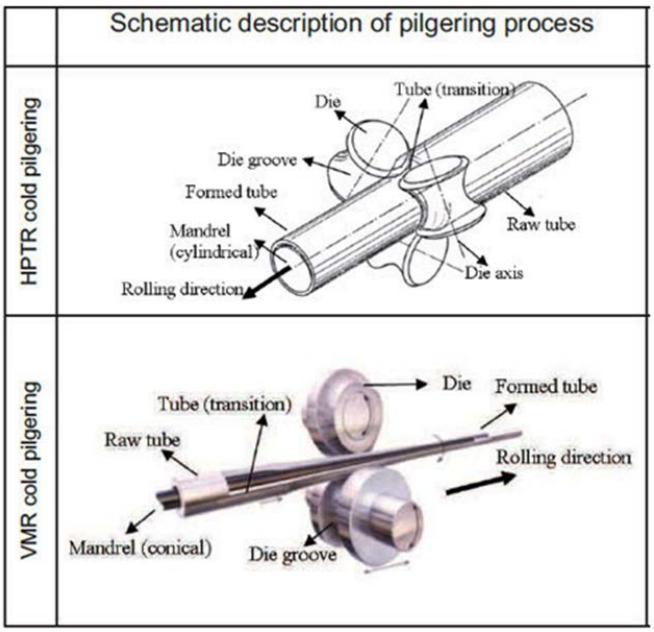

Figure 3. Commercial thin-wall tube fabrication processes through pilgering [20]. (HPTR = high-precision tube roller; VMR = vertical mass ring die).

3. POTENTIAL FAILURE POINTS DURING TUBE PRODUCTION

Failed C26M tubes are shown in Figure 4, which illustrates various types of failures during tube production, such as crack initiation and propagation near the shoulder of the pointing, a circumferential rupture in the middle of the drawn tube, and premature failure at the inside of the pointing region. The major type of failure was crack propagation along the tube axial direction, which ruined the whole length of the master tube. However, it should be emphasized that even after crack propagation, the wall thickness reduction was completed to achieve the original target wall thickness without forming additional defects, such as internal cracks. This indicates that the material is still deformable, and only crack initiation is an issue. Hereinafter, the potential failure points during the tube production processes are discussed to discover the optimized process conditions for production.

Figure 4. C26M tube failures during tube drawing process. The tube ODs are approximately 0.9 in.

3.1 Heat production process

As mentioned earlier, the as-cast VIM ingots of FeCrAl alloys tended to show hot cracks in the middle of the ingot, and HIP (at 1200°C/15 ksi/4 h) could successfully eliminate such internal defects. Figure 5 represents cross-sectional views of the as-cast VIM ingot (C06M2) and HIPed ingot (C26M). The cracks in the as-cast ingot could not be identified from visual inspection but became visible after sectioning of the ingot. If the cracks remained, the cracks appear on the external surface of the machined billets and they are exposed at elevated temperatures during soaking for the extrusion process (or any other master bar production process), resulting in becoming pathways for the formation of internal oxides along the cracks. Such oxides would act as other crack initiation sites during the subsequent production steps. Besides HIP, there are several different approaches to avoid such issues: use the “near net shape” as-cast ingot as an extrusion billet, seal the machined billets into a steel can, weld-repair the cracks on the machined billets, and so on. However, any of those methods retains the cracks internally before applying extrusion, so HIP is the best choice if it is applicable. Figure 6 shows pictures of HIPed C26M ingots and the machined billets. No cracks were observed on the billet ends from visual inspection.

If HIP were not feasible for technical reasons, another approach would be to gun-drill the center of the ingot and then fill another core material in the center hole or use tube extrusion with a mandrel.

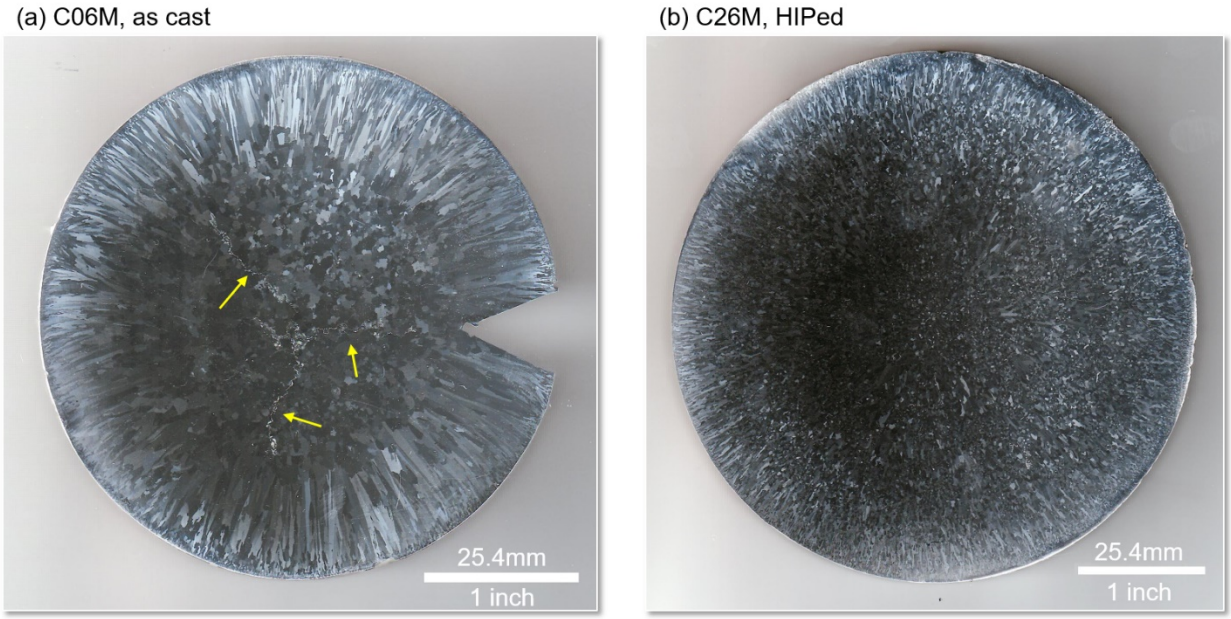

Figure 5. Cross-sectional views of Gen II. FeCrAl alloy VIM ingots; (a) as-cast C06M and (b) HIPed C26M. The arrows in the picture indicate solidification cracks existing only in the as-cast ingot. The arrows indicate the internal cracks formed after solidification.

Figure 6. (a) As-received C26M VIM ingots on which HIP was applied at 1200°C/15 ksi/4 h and (b) the machined billets of C26M ingots to be extruded.

3.2 Master bar production process

Hot extrusion is a commercially available bar production process. The extrusion process has two aspects to control the quality of the master bars: (1) producing a bar with a targeted diameter and sufficient length to be suitable for the subsequent tube reduction (drawing) process and (2) controlling the microstructure to produce a fully recrystallized, equiaxed grain structure with sufficiently refined grains below ~100 μm. Additional annealing may be required to further control the microstructure. The bar size depends on the subsequent tube drawing process, since the required initial OD (and WT) may vary with the expected total thickness reduction and the capability of the tube drawing manufacturers. The area reduction ratio (9.8 for the present extrusion process) needs to be in a certain range from the microstructure and quality control viewpoints. For example, a low reduction ratio (~4 or below) may result in the solidification microstructure remaining coarse and not being fully recrystallized; and too high a reduction ratio combined with a relatively low temperature would lead to a rough surface finish and the formation of "wrinkles." These could remain as hairline cracks near the surface (see Section 3.2) and become a source of premature failure during the subsequent tube reduction process.

Figure 7 illustrates parts of the master bar production process conducted at ORNL: hot extrusion, sectioning, straightening, and final annealing. The extrusion process should not be a major source of premature failure once an optimized temperature and area reduction ration are selected. On the other hand, straightening could easily cause transverse cracking at room temperature because of the limited deformation ability of FeCrAl alloys. Warm straightening at a temperature range of 200–300°C helps avoid such crack formation because it improves the ductility. It should be emphasized that exposure to that temperature range could lead to the formation of brittle BCC-Cr (alpha-prime), although the soaking time during straightening is short enough to ignore such microstructural changes.

Figure 7. Pictures of master bar production at ORNL; (a) a C26M bar just after extrusion, (b) the extruded bars during cooling, and (c) the bars after sectioning and straightening.

Figure 8 shows cross-sectional optical micrographs of an as-extruded C26M bar. The extruded bar exhibited an equiaxed, fully recrystallized grain structure near the bar surface, including the area to become a master tube after gun-drilling (Figure 8a, b). A scanning electron microscopy (SEM)/ electron backscatter diffraction (EBSD) analysis indicated that the fully recrystallized area consisted of randomly oriented grains with almost no texture formation, as shown in Figure 9a. This finding suggests that the area was crystallographically anisotropic and suitable for applying deformation in the tube reduction process. On the other hand, nonrecrystallized, deformed coarse grains remained near the center of the bar

(Figure 8c and Figure 9b). They were due to inhomogeneous material deformation during extrusion (i.e., a large shear strain was imposed near the surface area, whereas only monotonic compression or pushing was applied to the center area). Since the area near the center was not used in the final tube product, no additional annealing for the nonrecrystallized microstructure was applied.

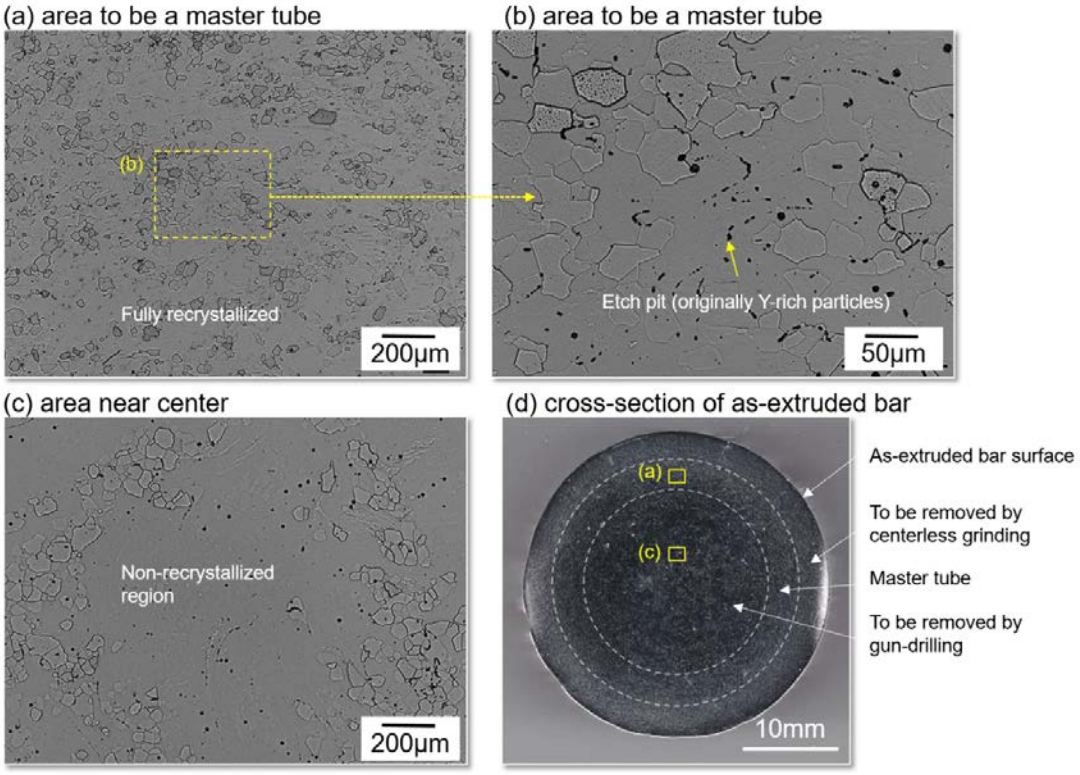

Figure 8. Light optical micrographs of an as-extruded C26M bar; (a, b) the area to become a master tube, (c) the area near the center to be removed by gun-drilling, and (d) a macroscopic cross-sectional view of the as-extruded bar after etching.

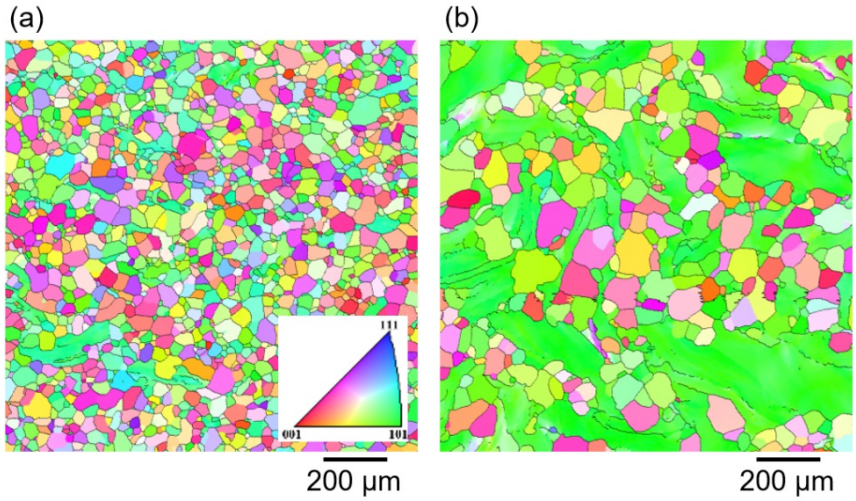

Figure 9. IPF color maps showing the crystallographic orientation of each grain obtained from SEM-EBSD analysis; (a) the area to become a master tube, and (b) the area near the center to be removed by gun-drilling.

Figure 10 shows cross-sectional optical micrographs of the fully recrystallized area in the C26M extruded bar before and after additional annealing at a temperature range from 800 to 1000°C. All materials were annealed for 30 min, followed by air cooling. It appears obvious that the higher the annealing temperature, the coarser the grain size. The average grain size was ~30 μm for the as-extruded condition and became ~50, 80, and 150 μm after annealing at 800, 900, and 1000°C, respectively. The Vickers hardness (HV) was ~240 HV after annealing at 800°C and ~220 HV after annealing at 900 and 1000°C. Previous studies [22] indicate that the area at 240 HV was not fully annealed and might have limited deformability at room temperature, whereas the area at 220 HV would be soft enough to subject to the tube reduction process. Room-temperature tensile property evaluation of the other Gen. II FeCrAl alloys, C36M2 (13Cr-6Al-2Mo base) and C36N3 (13Cr-6Al-0.7Nb base) [25], indicated that not only the yield and tensile strengths but also the ductility decreased with increasing average grain size, as shown in Figure 11. Less strength meant low deformation resistance, which was preferred for the tube reduction process, although larger grain sizes than ~130 μm also resulted in very little plastic elongation to rupture. Although the tensile ductility cannot be converted directly to the applicable area reduction during tube reduction process, it seems obvious that grain coarsening to greater than ~130 μm needs to be avoided to prevent unexpected failures during the subsequent process.

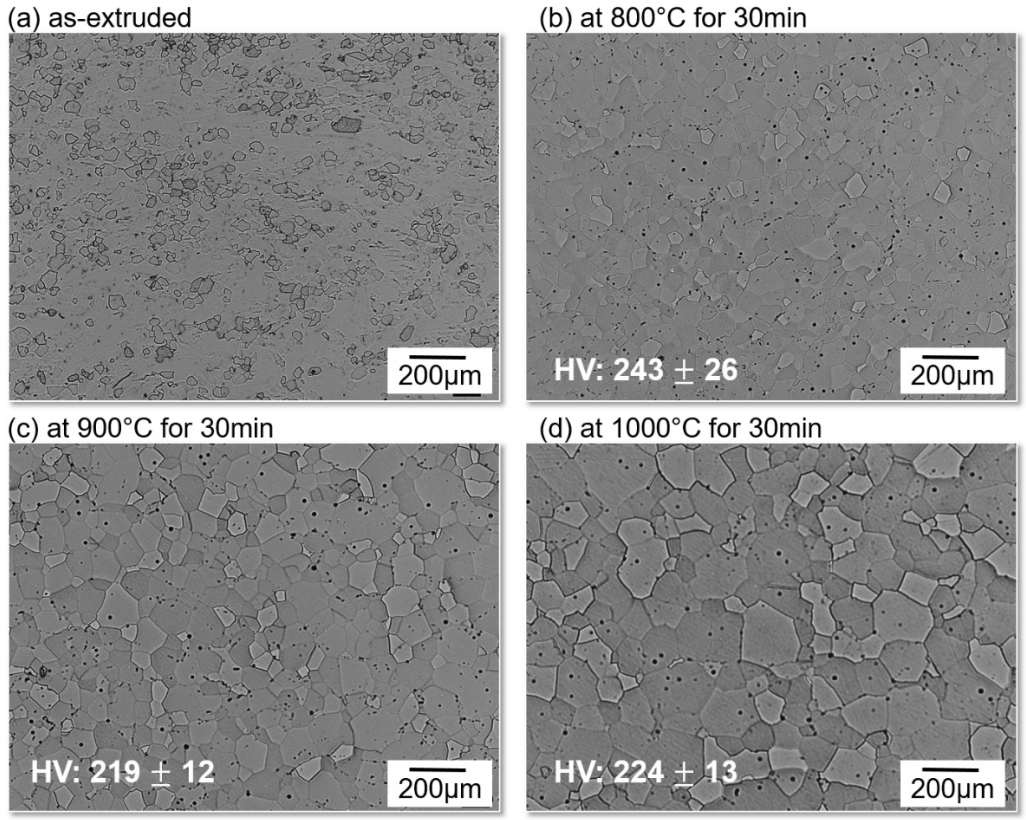

Figure 10. Light optical micrographs of the extruded C26M bar before and after annealing; (a) as-extruded, (b) annealed at 800°C for 30 min, (c) at 900°C for 30 min, and (d) at 1000°C for 30 min.

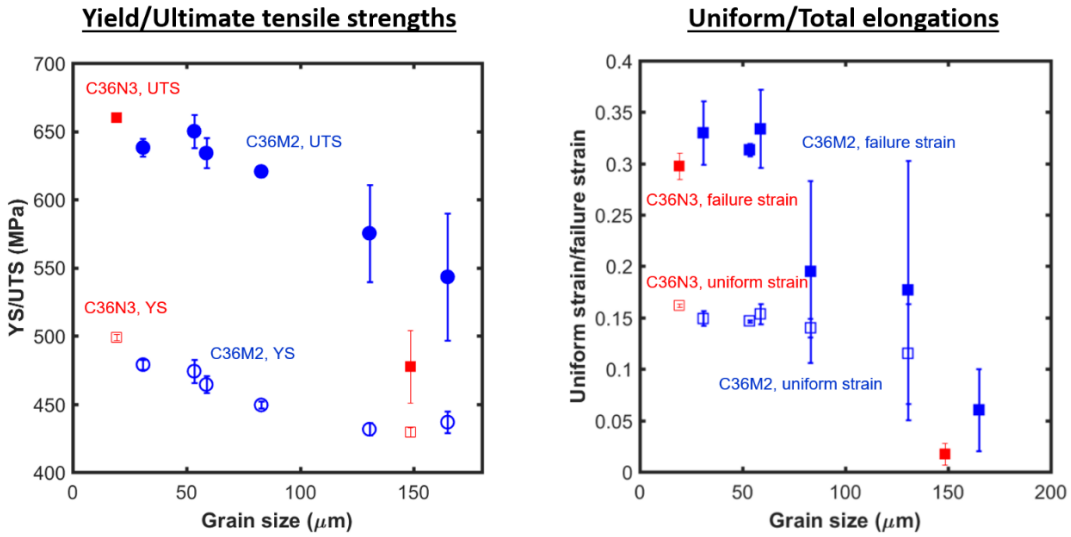

Figure 11. Room-temperature tensile properties of the Gen. II FeCrAl alloys C36M2 (13Cr-6Al-2Mo base) and C36N3 (13Cr-6Al-0.7Nb base) plotted as a function of average grain sizes [25].

Based on the findings discussed above, the extruded bars were annealed at 900°C for 30 min and then centerless-ground to prepare the master bars, as shown in Figure 12a. After visual inspection, 2 of 18 machined bars were found with external defects like hairline cracks (Figure 12b). Ultrasonic testing indicated the cracks exist only near the bar surface and the bar end and have limited lengths. The mechanism by which such cracks were formed was unclear, although it was speculated that surface wrinkles formed during hot extrusion could be the source. This could occur if the hot extrusion temperature was locally too low and ductile deformation near the surface was prevented. The results indicated that insulation of the billets to be extruded might help avoid the formation of such defects.

Figure 12. Machined C26M bars; (a) as-received bars, and (b) a hairline crack found at one end of the machined bar.

3.3 Tube reduction process

The master bars were gun-drilled to make master tubes for the tube reduction process. Figure 13 shows a photograph of a FeCrAl alloy master bar and tube to be drawn by a tube drawing manufacturer. The gun-drilling was performed by the tube drawing manufacturer as well. The constant wall thickness was the key to obtaining a uniform reduction process, so the size tolerance of the gun-drilling (and the straightness of the master bar) needed to be strictly controlled.

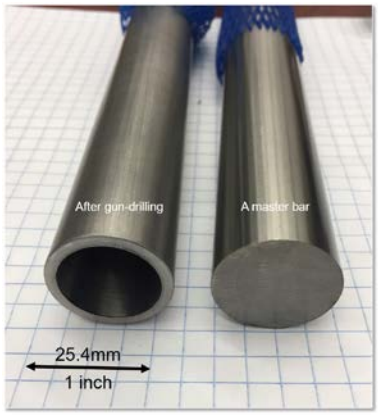

Figure 13. A picture showing a master bar before and after gun-drilling.

3.3.1 Annealing after drawing

To optimize the inter-pass annealing conditions, a C26M tube was annealed under various conditions after tube drawing with a 10% area reduction. An as-drawn C26M tube was provided from Century Tubes Inc. (San Diego, California), as shown in Figure 14; and the tube was sectioned into small pieces for the annealing study at 850 and 900°C for up to 60 min, followed by air cooling.

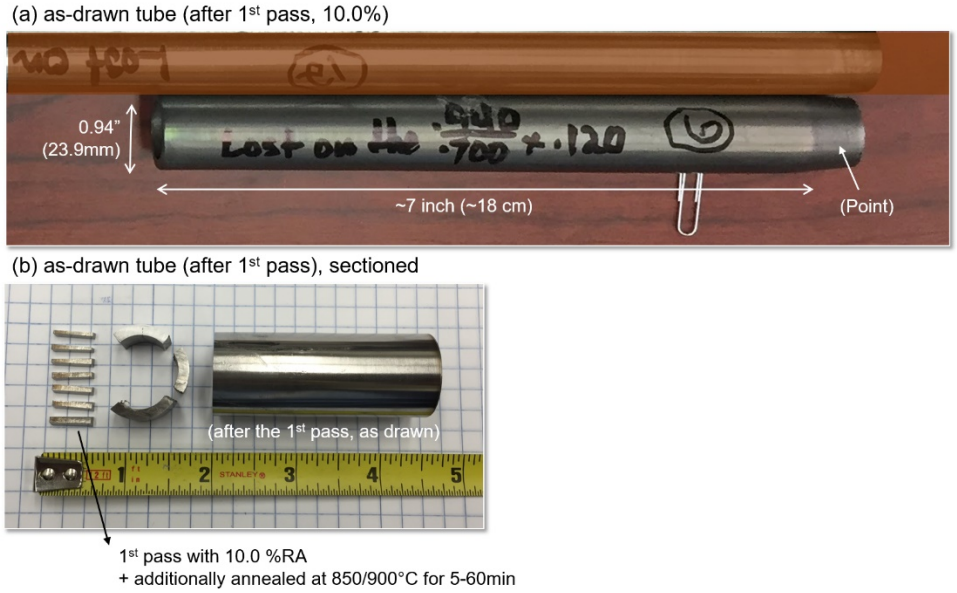

Figure 14. Pictures of a C26M tube after the first drawing pass with a10.0% area reduction; (a) an as-drawn tube with the point, and small pieces sectioned from the as-drawn tube for the annealing study.

Macroscopic grain structures before and after annealing are shown in Figure 15. All images were taken from the longitudinal section of the tube. The grain size in the as-drawn tube was ~80 µm, and there were few obvious changes in the grain size after annealing at 850°C for up to 60 min. Tubes annealed at 900°C also showed no significant changes for up to 15 min, whereas coarse grains larger than 200–300 µm became dominant after 30 min. The hardness values dropped from the as-drawn (~280 HV) to the annealed tubes (~210–230 HV), as shown in Figure 16. The hardness after annealing at 850°C gradually decreased as the annealing time increased, although it took 60 min to obtain a hardness value lower than 220 HV. On the other hand, annealing at 900°C produced the lowest hardness after 30 min, and then the hardness began to increase somehow after longer time exposure.

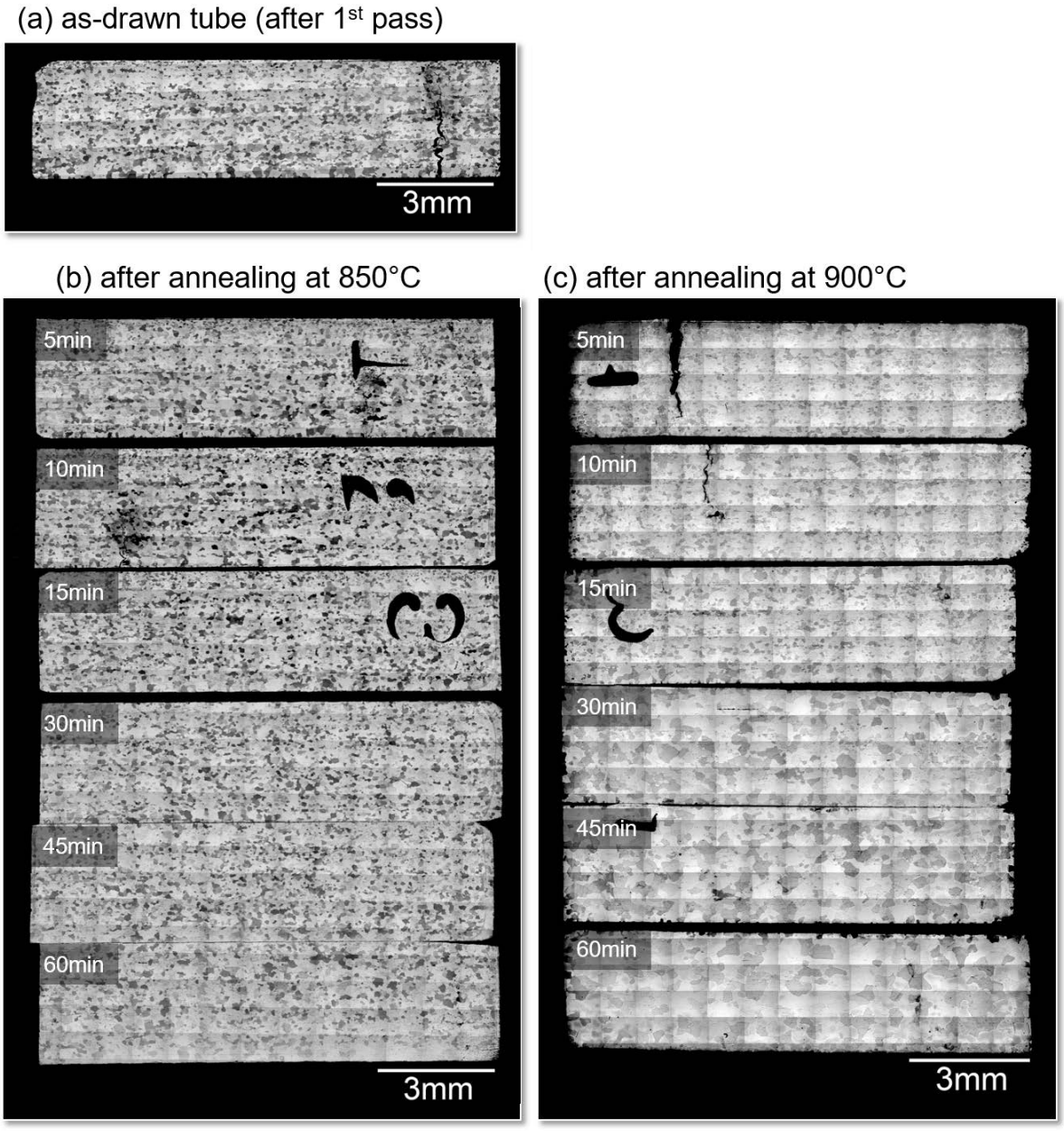

Figure 15. Macrostructures of sectioned pieces of the drawn C26M tube before and after annealing; (a) as-drawn, (b) after annealing at 850°C, and (c) at 900°C for up to 60 min.

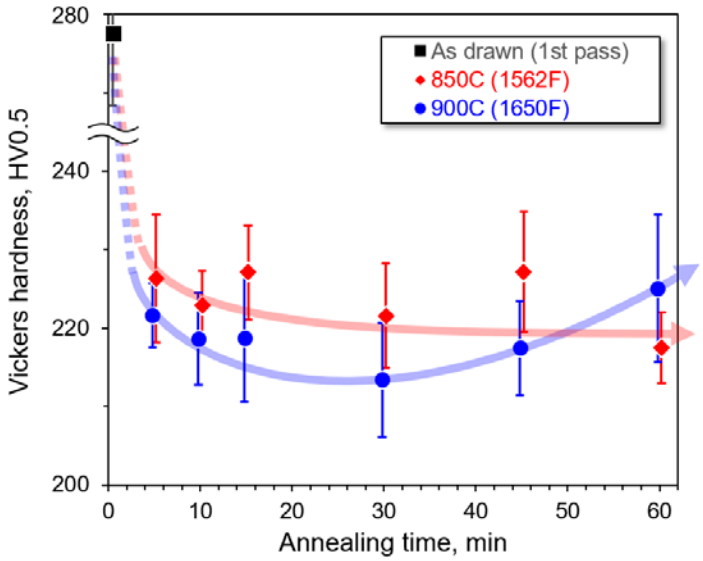

Figure 16. Changes in the hardness of a C26M drawn tube with annealing at 850 and 900°C.

The room-temperature tensile properties of the selected annealed tubes are summarized in Table 2. The uniform plastic strain was at the maximum after annealing at 900°C for 30 min, although the coarse grain formation shown in Figure 15 may not be suitable for better deformability. Based on these results, annealing at 900°C for 15 min was selected for the early stage of the tube reduction process.

Table 2. Room-temperature tensile properties of C26M drawn tube after annealing

C26M Century tubes, first pass 30min@850°C, 10^{-3} s^{-1}				
Test #	YS (MPa)	UTS (MPa)	Uniform strain (%)	Failure strain (%)
1	525	593	8.9	11.6
2	468	611	12	25.3

C26M Century tubes, first pass 15min@900°C, 10^{-3} s^{-1}				
Test #	YS (MPa)	UTS (MPa)	Uniform strain (%)	Failure strain (%)
1	477	613	11.5	23.2
2	478	595	11	24.3

C26M Century tubes, first pass 30min@900°C, 10^{-3} s^{-1}				
Test #	YS (MPa)	UTS (MPa)	Uniform strain (%)	Failure strain (%)
1	445	589	13.2	17.4
2	447	618	14.4	26.1

Another concern emerged during the annealing process: a dimple-like surface texture formed after the fourth drawing pass of the tube (Figure 17). The dimple size corresponded to the grain size, indicating that coarse grains are another issue associated with the surface quality of the as-drawn tube. The further thickness reduction and inter-pass annealing eliminated the formation of the dimple texture, possibly as a result of grain refinement. Therefore, grain size control during the tube reduction process also must be considered as a quality control parameters.

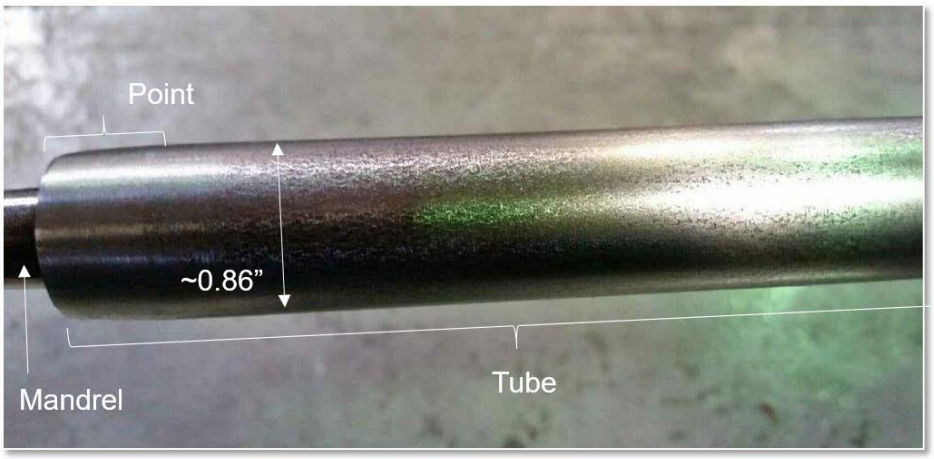

Figure 17. Drawn tube after four pass, showing a surface texture reflecting the presence of coarse grains.

3.3.2 Crack initiation during drawing

Figure 18 shows various C26M tubes that failed because of crack propagation along the tube axial direction. It was found that all cracks initiated near the shoulder of the pointing region (the tube end with a reduced diameter). Cross-sectional observation of the cracked tube (Figure 19) indicated that most of the cracks formed as transgranular failures, and there was no evidence that cracks propagated along any inclusions (e.g., oxide particles) or grain boundaries. As mentioned earlier (at the beginning of Section 3), the tube was successfully reduced to the wall thickness that was the original target, despite crack formation; that indicates that premature failure (i.e., cracking along the tube axial direction) is avoidable if crack initiation is prevented.

The as-drawn C06M2 tube with a 19.6% area reduction, provided by Superior Tube Company (Figure 20), also shows crack propagation along the tube axial direction. Three different cracks were observed at the tagged region, and all cracks seemed to initiate from the end of the shoulder of the tagged region. The Vickers hardness analysis indicated that the very beginning of the drawn tube (i.e., the end of the tagged region) was heavily work-hardened, as can be seen in the cross-sectional view of the tube and the contour map of the hardness in Figure 21. The work hardening was due to overlapping of the deformed regions from both tagging and drawing at the end of the tagged region, and it increased the susceptibility to crack initiation. One way to prevent crack initiation is to apply additional annealing at a relatively mild condition. Annealing at 800°C for 15 min successfully reduced the hardness of the tagged regions significantly, as shown in the upper side of Figure 21; it should reset all work hardening in the region and reduce crack susceptibility without leading to undesirable grain coarsening.

Figure 18. Failed C26M drawn tubes with cracks initiating near the shoulder of the pointing end.

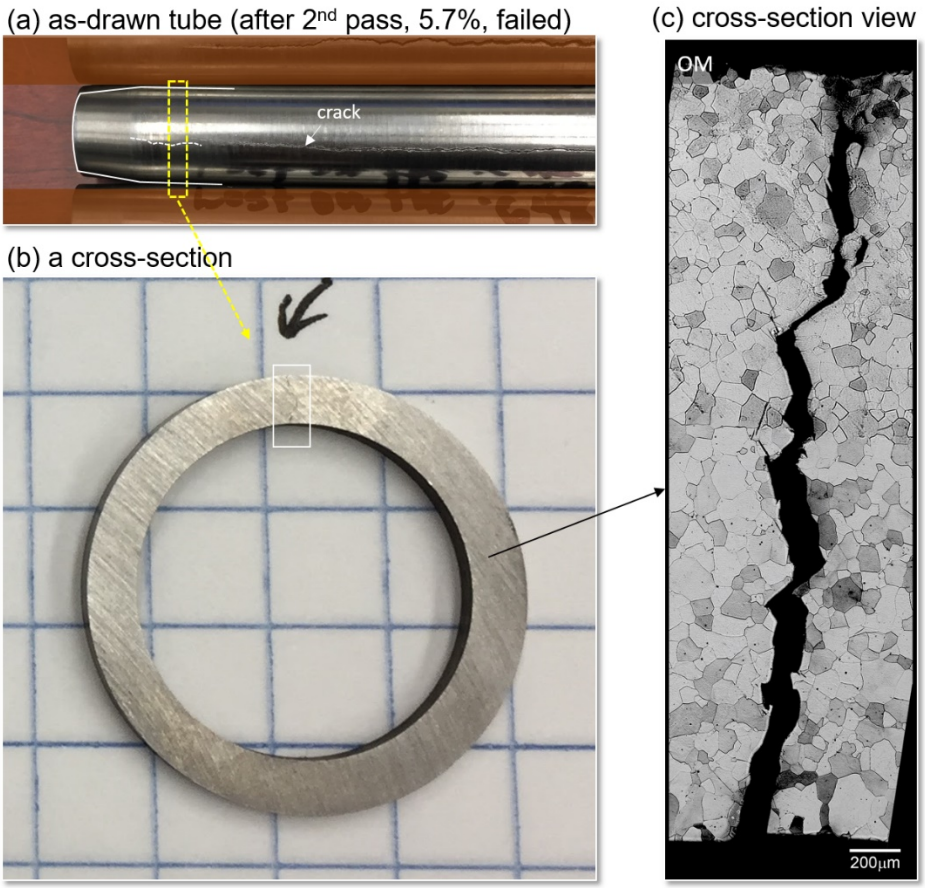

Figure 19. As-drawn C26M tube with 5.7% area reduction; (a) the tube with a crack along the tube axial direction, (b) a sectioned piece of the as-drawn tube, and (c) a light optical micrograph of the cross-sectional view near the crack.

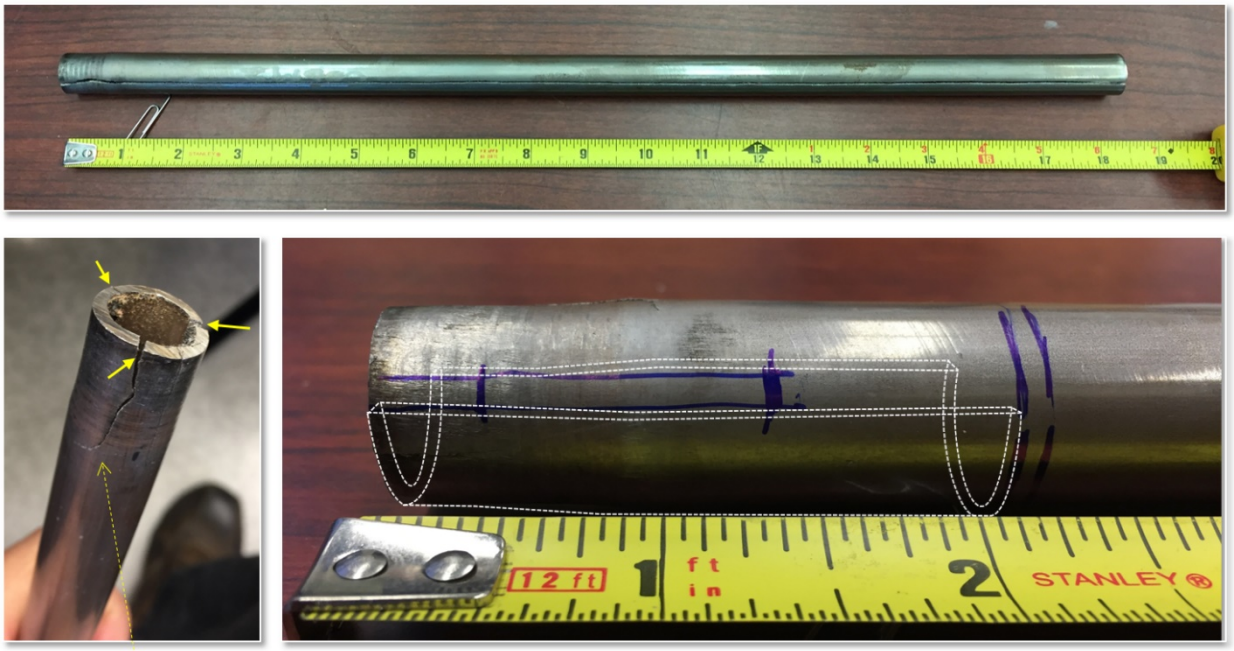

✓ Crack seems initiated from the shoulder.

Figure 20. As-drawn C06M2 tube with 19.6% area reduction showing cracks formed near the tagged region, together with the sectioning plan of the tube for metallographic characterization.

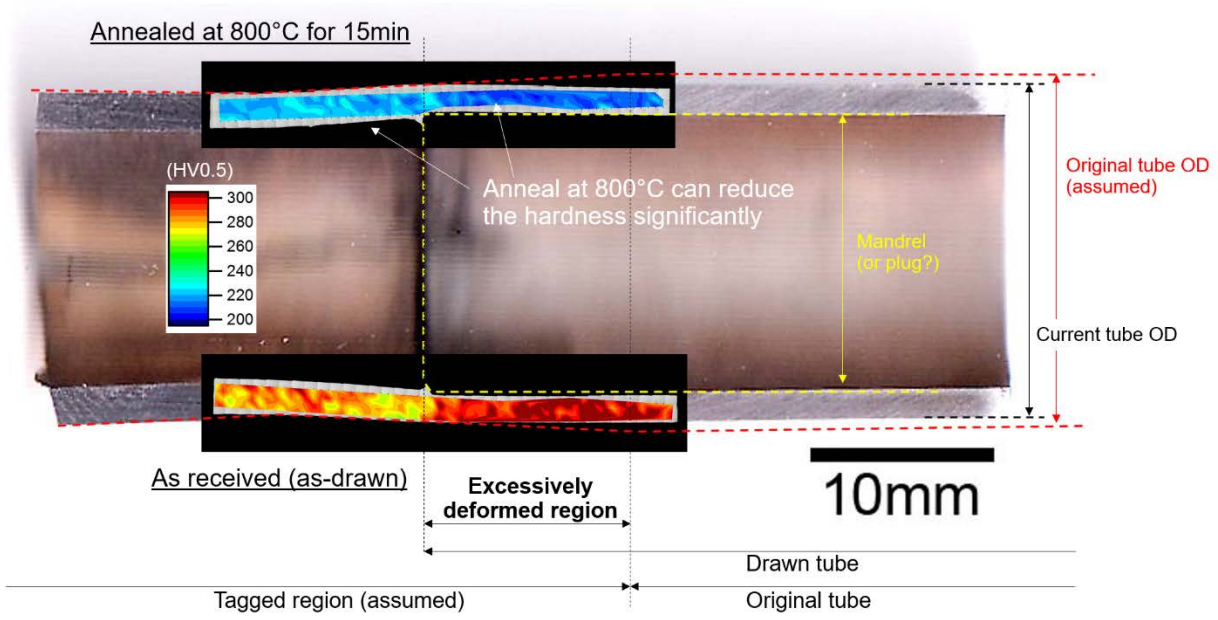

Figure 21. A cross sectional view of the tube with the tagged region, together with superimposed contour maps of Vickers hardness before and after annealing at 800°C for 15min.

4. TUBE PRODUCTION TO DATE

C26M tube production was initiated in FY 2017 and two different batches were produced. The first batch experienced many premature failures during the tube reduction process, which resulted in the delivery of tubes with limited lengths (~40 ft) and it was shorter than that originally expected from the provided master bars (1 in. diameter × 20 in. length, a total of nine bars). After the process parameters were optimized based on the findings discussed above, the second batch resulted in the production of tubes with a total length of ~170 ft, a more than 4× improvement in the material yield (Figure 22).

Figure 22. C26M tubes; (a) the first batch delivered at ORNL and (b) the second batch completed and to be delivered.

The cross-sectional characterization results are summarized in Figure 23, which indicates that the as-received (as-drawn) tube consisted of a fully recrystallized grain structure (with a certain amount of deformation due to the as-drawn condition) with an average grain size of ~60 µm. The measured wall thickness from the cross-sectional view was in the range of 397 to 405 µm, which was within the target tolerance (400 µm ± 25 µm). It would be important to control the grain size to be sufficiently small compared to the wall thickness during the tube reduction process, which allowed macroscopically uniform deformation, and therefore, the uniform wall thickness in the final tube products.

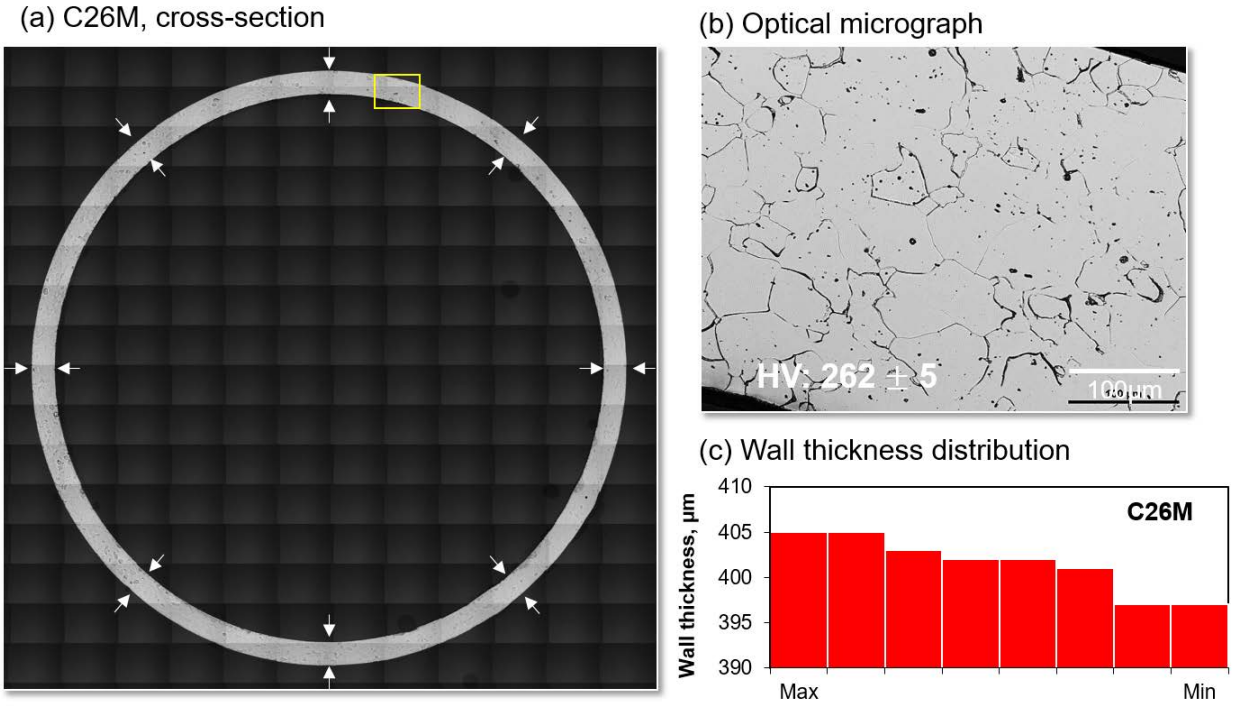

Figure 23. Cross-sectional macro- (a) and micrographs (b), together with the wall thickness distribution (c) of the as-received C26M tube.

5. SUMMARY

This report summarizes the various process parameters and conditions that triggered premature failures during the production steps for Gen. II ATF FeCrAl seamless tubes during a commercially available manufacturing process. It suggests optimized processing routes and parameters to improve the quality and the material yield of tube production. The production processes were divided into three major steps: (1) heat production, (2) master bar production, and (3) tube reduction. The detailed steps and potential failure points were discussed.

For heat production, not only chemical composition control but also the elimination of solidification defects in the VIM ingot were key. A hot-isostatic press helped reduce and eliminate internal, pre-existing cracks in the ingot that could be a source of premature failure (e.g., crack initiation from oxide particles) in the latter part of the tube production process. Another approach would be to gun-drill the centers of the ingots to eliminate the defect region and then insert another core material or apply tube extrusion.

The master bars were produced by a hot-extrusion process. The area reduction ratio as well as the extrusion temperature (and additional annealing after extrusion) were keys to controlling the quality of the master bars and the grain structure. Because of the limited deformability of FeCrAl alloys, especially at ambient temperature, controlled uniform grain structure with relatively small grains were required at the beginning of the tube reduction process.

In the tube reduction (drawing) process, a relatively small amount of area reduction per pass combined with controlled inter-pass annealing was needed for a lower chance of failure, a highly uniform wall thickness, concentricity, and a good surface finish. It was found that the end of the pointing (tagging) region was subject to additional deformation at the beginning of the drawing process, which increased the cracking susceptibility and resulted in propagation of cracks along the tube axial direction. Relatively mild annealing after pointing successfully reduced the chance of premature failure and increased the material yield drastically.

Based on the knowledge of process conditions obtained, FeCrAl tube production with optimized process parameters is currently in progress. A part of the final tube production inventory was delivered in late June 2017. Cross-sectional microstructure characterization was completed; and the improved quality of the tubes, including the size tolerance and the controlled grain structure, was confirmed.

6. REFERENCES

[1] D. Powers and R. Meyer, Cladding swelling and rupture models for LOCA analysis, NUREG-0630; U. S. Nuclear Regulatory Commission: 1980.

[2] B. A. Pint, K. A. Unocic and K. A. Terrani, Materials at High Temperature, 32 (2015) 28-35.

[3] M. Moalem, D. R. Olander, Journal of Nuclear Materials 182 (1991) 170.

[4] K. Suzuki, S. Jitsukawa, N. Okubo, F. Takada, J. Nucl. Eng. and Design 240 (2010) 1290–1305.

[5] M. Steinbrück, M. Große, L. Sepold, J. Stuckert, Nuclear Engineering and Design 240 (7) (2010) 1714-1727.

[6] Y. Yamamoto, B. A. Pint, K. Terrani, K. G. Field, L. L. Snead, "Letter report documenting identifying billets and alloys fabricated for distribution to program" M3FT-13OR0202291, ORNL/LTR-2013/322, Oak Ridge National Laboratory (2013).

[7] P. Grobner, Metallurgical and Materials Transactions B, 4 (1973) 251-260.

[8] K. G. Field, X. Hu, K. C. Littrell, Y. Yamamoto, L. L. Snead, "Radiation Tolerance of Neutron-Irradiated Model Fe-Cr-Al Alloys," Journal of Nuclear Materials, 465 (2015) 746-755.

[9] K.G. Field, M.N. Gussev, Y. Yamamoto, L.L. Snead, "Deformation behavior of laser welds in high temperature oxidation resistant Fe-Cr-Al alloys for fuel cladding applications," Journal of Nuclear Materials, 454 (2014) 352-358.

[10] B. A. Pint, S. Dryepondt, K. A. Unocic, and D. T. Hoelzer, JOM, 66 (2014) 2458-2466.

[11] Y. Yamamoto, Y. Yang, K.G. Field, K. Terrani, B. A. Pint, and L. L. Snead, "Letter Report Documenting Progress of Second Generation ATF FeCrAl Alloy Fabrication, FY14 FCRD milestone report," M3FT-14OR0202232, ORNL/LTR-2014/219, Oak Ridge National Laboratory (2014).

[12] Y. Yamamoto, M. N. Gussev, B. K. Kim, T. S. Byun, "Optimized properties on base metal and thin-walled tube of Generation II ATF FeCrAl", M2FT-15OR0202291, ORNL/TM-2015/414 (2015).

[13] Y. Yamamoto, "Development and Quality Assessments of Commercial Heat Production of ATF FeCrAl Tubes", M2FT-15OR0202252, ORNL/TM-2015/478 (2015).

[14] B. A. Pint, K. A. Unocic, K. A. Terrani, "Steam Oxidation of FeCrAl and SiC in the SATS", M3FT-15OR0202342, ORNL/LTR-2015/417 (2015).

[15] K. A. Terrani, S. J. Zinkle, L. L. Snead, "Advanced Oxidation-resistant Iron-based Alloys for LWR Fuel Cladding," Journal of Nuclear Materials, 448 (2014) 420-435.

[16] N. R. Brown, M. Todosow, and A. Cuadra, "Screening of Advanced Cladding Materials and UN–U3 Si5 Fuel," Journal of Nuclear Materials 462 (2015): 26-42.

[17] N. M. George, K. Terrani, J. Powers, A. Worrall, I. Maldonado, Neutronic analysis of candidate accident-tolerant cladding concepts in pressurized water reactors, Ann. Nucl. Energy. 75 (2015) 703–712.

[18] H. Qu, Y. Lang, C. Yao, H. Chen, C. Yang, Materials Science and Engineering: A 562 (2013) 9-16.

[19] "Shanghai EverSkill M&E Co., Ltd": *http://www.esmeind.com/Pro-Tube.html#*

[20] "Cold Pilger Rolling: Part One," website of Total Materia, Apr. 2013: *http://www.totalmateria.com/page.aspx?ID=CheckArticle&site=kts&NM=396*

[21] A. Nerino, M. Deaver, C. Nagele, J. Reinhart , "HPTR's past, present, and future—Part I," TPJ—The Tube & Pipe Journal, Jun. 2011: *http://www.thefabricator.com/article/tubepipeproduction/hptras-past-present-and-future-a-part-i*

[22] Y. Yamamoto, Z. Sun, M. N. Gussev, B. A. Pint, K. A. Terrani, "Examination of Compressive Deformation Routs for Production of ATF FeCrAl Tubes," M3FT-16OR0202133, ORNL/TM-2016/509 (2016).

[23] Y. Yamamoto, Z. Sun, B.A. Pint, K.A. Terrani, “Optimized Gen-II ATF FeCrAl cladding production in large quaontity for campaign testing”, M3FT-16OR020202132, ORNL/TM-2016/227 (2016)
[24] Z. Sun and Y. Yamamoto, Processability evaluation of a Mo-containing FeCrAl alloy for seamless thin-wall tube fabrication. Materials Science and Engineering: A, 2017. 700: p. 554-561
[25] Z. Sun, Y. Yamamoto, “Microstructural control of FeCrAl alloys using Mo and Nb additions” submitted to *Materials Characterization* (2017).